Hamed *et al.*
Progress in Earth and Planetary Science (2022) 9:35
https://doi.org/10.1186/s40645-022-00494-3

Progress in Earth and Planetary Science

RESEARCH ARTICLE Open Access

Climatic zonation of Egypt based on high-resolution dataset using image clustering technique

Mohammed Magdy Hamed[1*], Mohamed Salem Nashwan[2] and Shamsuddin Shahid[3]

Abstract

Egypt, a predominantly arid and hyper-arid country, is one of the environmentally most fragile regions of the world. The country became a hot spot for climatic extremes and aridity change in the global warming context. The unavailability of a detailed and reliable climate zonation map is a major hindrance to climatic studies in Egypt. This study attempted to generate a high-resolution climate zone map of Egypt based on a novel image analysis technique. For this purpose, a colored image representing Egypt's composite climatology was developed using three high-resolution (1-km) climate variables: rainfall, maximum temperature and minimum temperature during 1979–2013. A spherical evolution algorithm was used to classify the image into different climate zones. Subsequently, the climate zones representing similar climate distribution were merged to generate the climate map of Egypt. The study revealed that Egypt's distinguishable climate zones could be recognized when the land area was classified into nine zones using the image analysis technique. The statistical analysis of climate variables of each zone revealed similar climatology only in two pairs of zones. The merging of similar climate zones yielded seven climate zones having distinct climate characteristics. The validation of climate zonation using various statistical tests revealed the robustness of the proposed method in classifying climate. The climate zone map generated in the study can be used as a reference for climate change analysis in Egypt.

Keywords: Egypt, Climate zone, Spherical evolution, Data clustering optimization, Image clustering

1 Introduction

Climate defines ecology, species distribution, water availability, land suitability for cropping, irrigation needs, harvesting scheduling and prevalence of diseases in an area (Belda et al. 2014; Trewartha and Horn 1980). Therefore, climate classification has paramount importance for regional development planning. The climate of an area is generally classified based on vegetation distribution as different species have a climatic niche (Bailey 2009; Feddema 2005). However, vegetation distribution data are unavailable in most parts of the world. Therefore, different climate variables like rainfall, temperature and humidity are mostly used for climate classification (Baker et al. 2010; Sa'adi et al. 2021). The selection of the climate variables depends on the target application of the climate classification and the spatial scale of the study area (Sihag et al. 2020; Tai et al. 2010).

Many studies have been conducted for global and regional climate classification (Belda et al. 2014; Hubalek and Horakova 1988; Netzel and Stepinski 2017; Sa'adi et al. 2021; Sánchez-García et al. 2020; Xiong et al. 2019). The studies used different classification schemes, such as Köppen (Köppen 1936), Köppen–Geiger (Geiger 1954), Thornthwaite (1948) and Köppen–Trewartha (Trewartha and Horn 1980). The existing classification scheme provides a broad climate classification of a region. For

*Correspondence: eng.mohammedhamed@aast.edu

[1] Construction and Building Engineering Department, College of Engineering and Technology, Arab Academy for Science, Technology and Maritime Transport (AASTMT), B 2401 Smart Village, Giza 12577, Egypt
Full list of author information is available at the end of the article

example, most parts of the Middle East and North Africa (MENA) belong to arid climate (BW) according to Köppen and Köppen–Trewartha climate classification scheme (Belda et al. 2014). However, rainfall and temperature in the BW zone in MENA significantly vary from place to place. Therefore, a more detailed land classification according to rainfall and temperature variability is vital for regional planning and economic activities.

In recent years, different methods have been proposed to classify climate at a regional scale (Bienvenido-Huertas et al. 2021; Netzel and Stepinski 2017; Sa'adi et al. 2021; Yanling et al. 2008). Those methods mostly classify the lands according to homogeneity in different climatic characteristics and, therefore, are considered more reliable for representing ecological distribution (Fávero and Belfiore 2019). Hubalek and Horakova (1988) used cluster analysis with Euclidean distance to evaluate the climate similarity in Europe. Sa'adi et al. (2021) used hierarchical (e.g., Ward's method) and non-hierarchical (e.g., *k-mean*) methods to define the climate zone of Borneo using a 0.25° spatial resolution climate dataset. Netzel and Stepinski (2017) classified the world's climate using the dynamic time warping similarity function. Among the methods, the cluster analysis, such as the newly developed spherical evolution algorithm (SEA) (Tang 2019), has been found more reliable as it can efficiently categorize individual locations based on their homogeneity and heterogeneity (Bienvenido-Huertas et al. 2021; Kaufman and Rousseeuw 2009; Sa'adi et al. 2021; Sánchez-García et al. 2020; Xiong et al. 2019). Tang (2019) compared ten clustering methods with SEA using six benchmark datasets and revealed that SEA has superior local and global search capabilities for solving unimodal and multidisciplinary optimization problems.

Generally, in situ observed climate data are used for climate classification. The quality of climate observations largely affects climate classification. However, reliable climate observation is not available or limited in many regions (Hamed et al. 2022c; Hamed et al. 2021; Salehie et al. 2021; Salman et al. 2019). Climate classification based on less quality or sparsely distributed observed data is prone to high uncertainty. Gridded climate data have been extensively used in recent years to overcome the challenge of data scarcity. The gridded climate data have also been used for climate classification. Kottek et al. (2006) first used gridded climate data of the climate research unit (CRU) for classifying the globe into different climate regions. In recent years, many other studies used gridded climate data to classify global and regional climates (Belda et al. 2014; Rubel and Kottek 2010; Sa'adi et al. 2021). The major challenge of climate classification using gridded data is that the spatial details of climate zones are limited to the resolution of gridded climate data. Most previous studies used gridded climate data with spatial resolutions ranging from 0.25° to 1.00° for climate classification (Belda et al. 2014; Sa'adi et al. 2021). Thus, it was not possible to provide climatic details below the resolution of the data used. However, a high-resolution climate classification is very important, particularly in arid regions, considering the limited availability of suitable land for agricultural, human settlement and other development activities.

Egypt, located in North Africa, is an arid country with inadequate available land for development activities. High aridity has made about 96% of Egypt a desert. Therefore, only a limited amount of land in the country is suitable for agricultural activities (AFED 2017; Collins et al. 2017). Egypt's population is over 100 million and growing by 2 million per year (Sweed 2016). Expansion of agricultural land and human settlement is essential to ensure food and housing for the growing population. A detailed evaluation of land according to climate can aid in identifying suitable land for agricultural development and establishing new settlements. Besides, Egypt's climate showed a rapid change in recent years (Gado and El-Agha 2021; Hamed et al. 2022a, b; Nashwan and Shahid 2022). The maximum temperature has increased from 0.07 to 0.24 °C/decade and the minimum temperature by 0.08–0.29 °C/decade in the last five decades (Nashwan et al. 2019b). At the same time, the rainfall decreased up to −5.00 mm/decade in the Nile Delta (Gado and El-Agha 2020; El Kenawy and Mccabe 2016; Nashwan et al. 2019c). The climate changes worsened the country's status of high-risk desertification (Abuzaid and Abdelatif 2022; Badreldin et al. 2014; Gad 2020). Therefore, the country must identify vulnerable climate zones to combat desertification.

In this study, a new methodology is presented to classify the recent (1979–2013) climate of Egypt based on the image clustering technique and SEA using the fine-resolution gridded climate data, Climatologies at high resolution for the earth's land surface areas (CHELSA). The SEA adopts a novel spherical search mechanism instead of the conventional hypercube search mechanism. This study is the first to adopt the SEA for climate classification. The climate zone map generated in this study could aid in deciding region-specific mitigation measures to combat Egypt's growing pressure on land resources. The method employed in this study can be replicated in any other region or on a global scale for a detailed and reliable climate classification.

2 Study area and data

2.1 Study area

This study covers Egypt, which is around (1,010,408 km^2) area. It is located on the edge of Africa and Asia,

within the geographic boundaries of latitude 22°–32° N and longitude 25°–35° E, as shown in Fig. 1. Egypt has the largest population within the MENA region. Generally, the climate of Egypt is relatively wet and cool in winter (October to March) and dry and hot in summer (April–September) (Nashwan and Shahid 2019a). The four seasons show geographical and temporal variety due to the country's significant regional and temporal variability in climate. Egypt's location and topography play a role in the distribution of rainfall and temperature. The rainfall in Egypt is relatively more in the coastal area along the Mediterranean Sea in the north (> 200 mm/year) and the Red Sea in the east than in the inland areas. Most areas in the south and west of Egypt, a part of the Sahara, receive an average rainfall of below 5 mm. Rainfall in the north is influenced by the North Atlantic Oscillation (NAO) (Elmallah and Elsharkawy 2011; Shaltout et al. 2013), Mediterranean Oscillation (MO) (Elmallah and Elsharkawy 2011; Hamed et al. 2021; Redolat et al. 2019) and the East Atlantic–West Russia index (Hasanean 2004). In contrast, the Red Sea through influences the east and south (Tsvieli and Zangvil 2007). Furthermore, temperature varies in Egypt by location and altitude. The temperature generally gets cooler in the north than in the south. The mean temperature in the north is around 20 °C, while 25.9 °C in the south. However, the temperature in higher elevation lands, such as Saint Catherine Mountain, may reach subzero in winter.

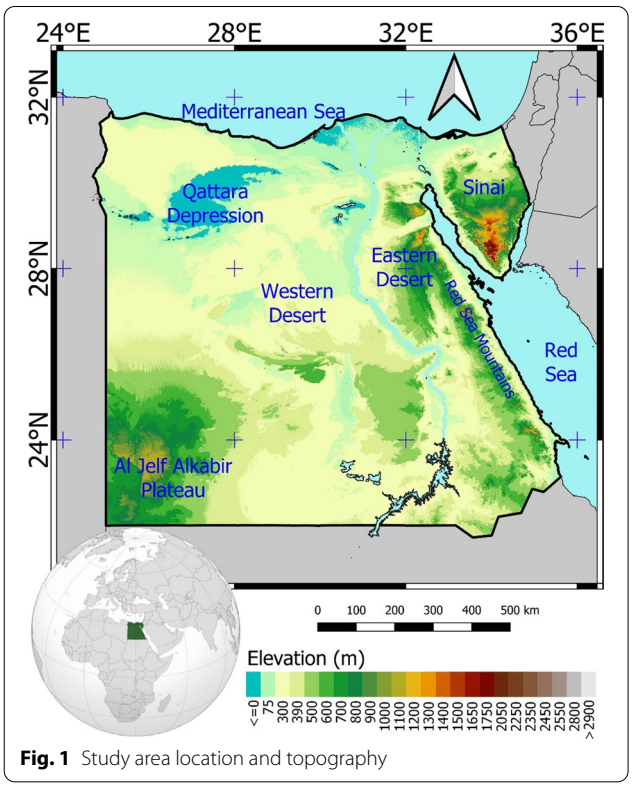

Fig. 1 Study area location and topography

2.2 Previous climate classification in Egypt

The review of existing literature suggests four climate zones in Egypt. A description of those classifications is provided in this section. The Köppen–Geiger climate classification method (Geiger 1954; Köppen 1936) categorized Egypt into three climate zones (Peel et al. 2007): dry semiarid with low latitude and altitude (BSh), dry arid with low latitude and altitude (BWh) and dry arid with mid-latitude and high altitude (BWk) (Fig. 2a). The Köppen–Geiger classification considered the climate of Egypt as mainly BWh and missed the distinctive details of the regional climate, which different researchers attempted to address later.

Secondly, few other studies also tried to classify the climate of Egypt. Ibrahim et al. (1994) presented a climatological classification of Egypt broadly into six different regions as shown in Fig. 2b: Mediterranean (MD), Nile Delta (ND), Middle Egypt (ME), Upper Egypt (UE), Red Sea (RS) and Sinai Mountains (SM). Thin strips along the Mediterranean and the Red Sea with high rainfall are defined as MD and RS, respectively, while SM is defined based on altitude. The remaining zones are defined based on temperature variation by latitude. A detailed description of each zone is provided in Nashwan et al. (2019a).

Another study classified Egypt's climate into eight zones (Fig. 2c): North Coast, East Coast, Delta and Cairo, Northern Upper Egypt, Southern Upper Egypt, Southern Egypt, Altiplano and Desert (HBRC 2006; Sayed et al. 2013). This classification is an updated version of the earlier climate zonation. It was proposed for engineering applications in the Egyptian Code of Practice for Enhancing Energy Use in Buildings. The classification is based on the mean temperature, rainfall, humidity, wind speed, solar radiation, altitude and physical terrain. However, it focused only on Egypt's occupied land, the Nile Delta and Valley, the coastal regions while classifying the rest of the land as 'Desert.' This classification neglected that the north and south of eastern and western deserts have distinct climatological characteristics. Besides, the Nile valley was climatologically divided between the east and the west without proper justification.

Lastly, Fig. 2d, e presents the agroclimatic classification proposed by Ouda and Norledin (2017) based on 10 (2005–2014) and 20 (1995–2014) years of potential evapotranspiration data, respectively. Both classifications were based on reference evapotranspiration (ET_o) for different study periods in different governorates. The calculation of ET_o was based on daily solar radiation, Tmax, Tmin, Tmean, wind speed and dew point temperature from meteorological stations. The main drawbacks of

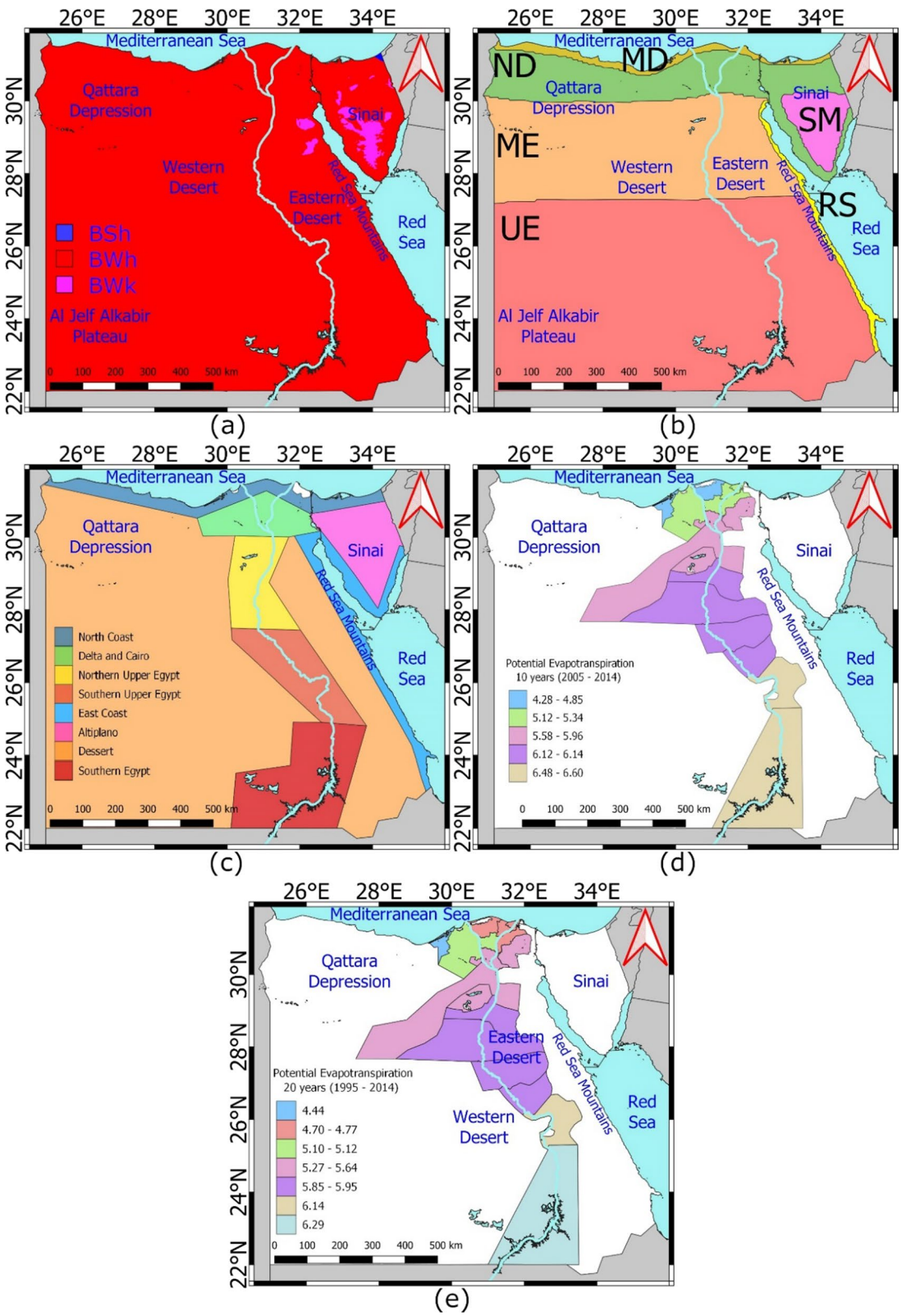

Fig. 2 Maps of previous studies on climate zoning of Egypt. **a** Köppen–Geiger climate classification. **b** Six climate zones for the whole land: Mediterranean (MD), Nile Delta (ND), Middle Egypt (ME), Upper Egypt (UE), Red Sea (RS) and Sinai Mountains (SM). **c** Eight climate zones for the whole land. **d**, **e** Agro-climate classification zones according to potential evapotranspiration for 10 and 20 years

these two classifications are: (1) the use of few meteorological records to represent a vast area; (2) the usage of the administrative boundaries as frontiers of each climate zone; and (3) the limited land coverage of these classifications as they focused only on the fertile land in the Nile Delta and Valley. This largely hindered their use, especially for future desert land reclamation and development. Several studies stated the importance of using a representable number of gauge records for a given area or catchment to minimize error in estimating the spatial characteristic of climate variability (Barbalho et al. 2014; Hwang and Ham 2013; Lee et al. 2013; Morrissey et al. 1995; Sharp et al. 1961; Zawadzki 1973).

Following observations can be made from the review of the previous classifications. Previous classifications mostly concentrate on the broad classification of Egyptian climate using sparsely distributed climate observation data. The frontiers of each zone were outlined based on administrative border or naive ingenuous vectors. Furthermore, they ignored the desert areas (nearly 96% of Egypt's land) and thus limited their usage only to occupied regions in Egypt, especially for the last three classifications. Furthermore, they also ignored the distinct climatological characteristics of the unoccupied regions as the Qattara depressions, which cover nearly 20 thousand km^2 area (El-Ramly 1965) and the Al-Jelf Alkabir Plateau, which receives the least rainfall in the Sahara Desert (Kelley 2014). Lastly, Egypt suffers from the lack of adequately distributed gauges leading to sizable areas being ungauged. The unavailability of in situ observations has limited the knowledge of the climatic characteristics of the country. This emphasizes using high-resolution gridded climate data to understand the regions' climatology and climate classifications.

2.3 Gridded rainfall and temperature dataset

CHELSA is a high-resolution (1-km) reanalysis of monthly gridded rainfall (R), maximum temperature (Tmax) and minimum temperature (Tmin) time series datasets for 1979–2013 generated by downscaling of ERA-Interim dataset (Karger et al. 2017). The mean monthly temperature was downscaled from ERA-Interim six-hourly monthly means of daily mean temperature data (Karger et al. 2017). The temperature was interpolated to sea level, then to grid cells, and finally projected back on the elevation obtained from the digital elevation model (DEM) (Karger et al. 2017). The minimum and maximum temperature at 2 m was calculated by climatological aided interpolation of three-hourly data of minimum or maximum temperature in ERA-Interim and B-spline interpolation of mean monthly temperatures (Karger et al. 2017).

For the rainfall, the influence of orographic predictors, such as boundary layer height, wind fields and valley exposition, was incorporated into the Global Precipitation Climatology Centre (GPCC) and Global Historical Climate Network (GHCN) datasets using a bias correction process (Karger et al. 2017). Some station data from GHCN, Federal Office of Meteorology and Climatology MeteoSwiss and Deutscher Wetterdienst (DWD) were used to correct the bias in the resulting data using a multilevel B-spline interpolation (Karger et al. 2017). A wind index was used to get the windward impact on rainfall intensity based on prevailing wind direction (Karger et al. 2017). For this purpose, the u-wind and v-wind components of ERA-Interim were interpolated by the B-spline method (Karger et al. 2017).

Previous studies found CHELSA v.1.2 as the most powerful high-resolution reanalysis gridded dataset in reproducing gauge observations for Egypt (Hamed et al. 2021; Nashwan 2020; Nashwan and Shahid 2019b). CHELSA showed significant correlations with NAO and MO in Egypt. It has a far higher spatial resolution than any gauge-based gridded climate data. It also provides both the rainfall and temperature time series. Therefore, CHELSA was selected and used in the present study. Figure 3 presents the spatial distribution of rainfall, T_{max} and T_{min} in Egypt as estimated by CHELSA.

3 Methodology

This study proposes a novel clustering method for climate zoning using an image classification method called spherical evolution algorithm (SEA). The flowchart presented in Fig. 4 describes the methodology of the proposed climate zoning method. In the proposed technique, T_{max}, T_{min} and rainfall were considered the three fundamental color bands of red, green and blue (RGB) to form a complete image, representing the climatology as discussed in Hamed et al. (2022b). These variables are the most influential factors for climate characterization (El-Geziry et al. 2021; Haque et al. 2015). Other climatic parameters directly or indirectly depend on either of them. The image classification algorithm initially considered a different number of climate zones. The climate zones were validated using multivariate analysis of variance (MANOVA) and probability density function (PDF) for selecting the suitable number of classes to present the climate in Egypt. The methodology is divided into five main steps, as described below.

3.1 Producing images

A colored image is the rendering of three bands, red, green and blue (RGB) conjointly. Each band contributes an image in a grayscale format. In the grayscale image, each pixel represents the brightness level. The byte image

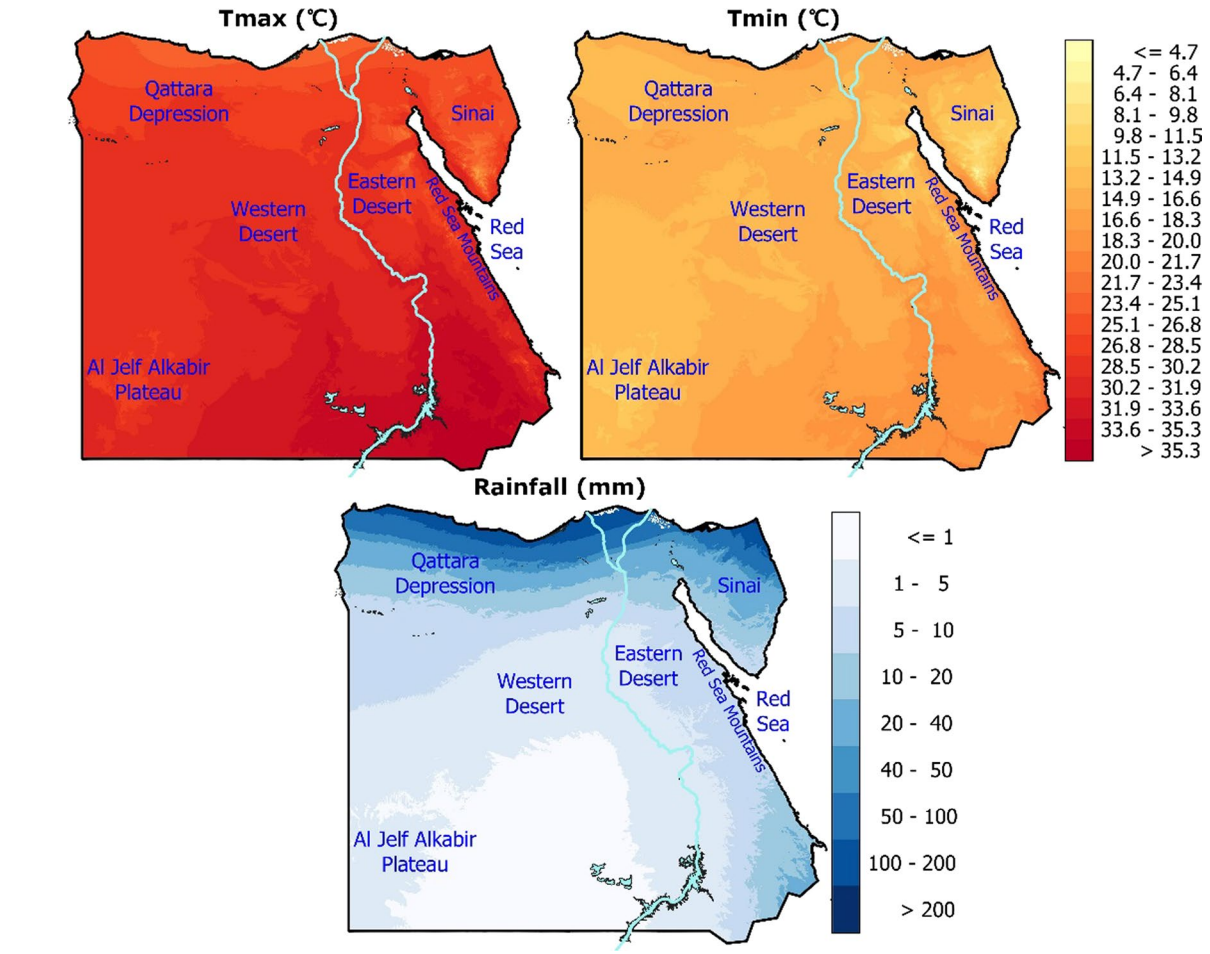

Fig. 3 Spatial variation in CHELSA maximum and minimum temperatures (°C) and annual mean rainfall (mm) over Egypt for 1979–2013

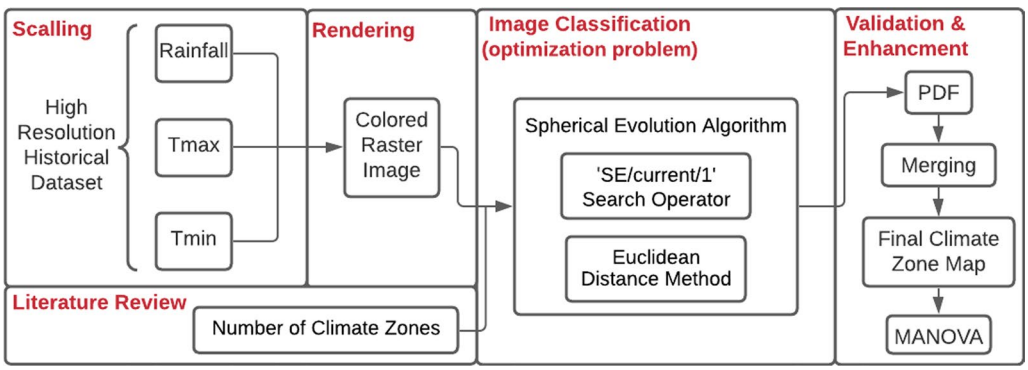

Fig. 4 Flowchart describing the methodology proposed in this study for climate zoning of Egypt

is the most common pixel format, where the pixel brightness is encoded as an 8-bit integer or as a value between 0 and 255. Pixels with a zero value mean zero visibility or black and pixels with a value of 255 indicate maximum brightness or white. Hamed et al. (2022a) proposed that this concept can be utilized to represent and visualize the climate of a given zone by scaling the values of rainfall, T_{max} and T_{min} between 0 and 255. For instance, a pixel

indicates the mean annual rainfall at the grid location in the greyscale image. As a result, the grids with higher rainfall are lighter than those with lower rainfall. The same process is applied for temperature greyscale images.

CHELSA grayscale images of T_{max}, T_{min} and rainfall were used as the three essential colors of red, green and blue (RGB), respectively, to form an image in the proposed procedure. Thus, the rendered RGB image can represent the composite climatology of Egypt. A few steps transform the values of each climate variable into a grayscale value. (1) Rainfall, Tmax and Tmin at each grid were converted into the annual average. (2) Then, the annual averages were rescaled to 8-bit integer using Eq. 1.

$$Y_i = \frac{[x_i - \min(x)] \times 255}{\max(x) - \min(x)} \quad (1)$$

where Y_i is the rescaled value of i grid, x_i is the grid value, and $\max(x)$ and $\min(x)$ are the max and min values of given climate variables found among the reanalysis gridded data. The scaling procedure makes the distribution of the original climate value the same as the output values. Finally, the three scaled bands were merged to form a complete colored image to visualize Egypt's climate as estimated by CHELSA for 1979–2013.

3.2 Image clustering

Most of the search styles clustering methods as K-means may fall into local optimum due to the initial selection of clusters centroid (Abidi et al. 2021). SEA, a nature-inspired meta-heuristic algorithm consisting of a spherical search style and search pattern (Tang 2019), is proposed to overcome this problem. The spherical search style can perform a more solid assessment than the hypercube search style, and it can be presented either as one-, two- or high-dimensional space ($\dim \geq 3$). The parameters of the spherical search style may require some tuning, and these parameters are the scale and dimension selection factors. By using Randomly Selection Method (RSM) and Designated Individual Selection Method (DISM) along with the search pattern equation and spherical search style equations, the 'SE/current/1' operator was chosen to image clustering as it showed the best performance in solving data clustering problems (Tang 2019). This operator has superior local and global search capabilities for solving unimodal and multidisciplinary optimization problems. Tang (2019) performed a real-world data clustering optimization problem.

As the output of the previous step was an image that visualizes Egypt's climate, the same concept of image classification could be used to identify the climate zones in Egypt. As a result, different zones defined by the SEA should have the highest variance against each other. Also, each zone should have data with the highest similarity and lowest distance to the centroid. The objective function of image clustering can be presented as:

$$\text{Min}J = \sum_{i=1}^{n} \sum_{j=1}^{k} d_{ij}(X_j - C_j)^2 \quad (2)$$

where X_j is the image data (3 bands), and C_j is the centroid of each zone, while $d_{ij}(X_j - C_j)^2$ is the distance between both parameters using the Euclidean distance method. The number of gridded data is n and k is the number of zones. The main objective function is to minimize the J by finding the best centroid for each zone. As the SEA needs an initial value of zone numbers (k), this study preliminary assumed that there could be six, seven, eight or nine climate zones based on previous climate classification in Egypt as presented earlier in Sect. 2.2. The classification of Egypt's climate into three zones based on the Köppen–Geiger climate is primitive. Thus, it was not considered the initial value of K. The climate zones prepared using each of the selected numbers were validated through visual inspection and statistical methods. The procedure is presented in the following subsection.

3.3 Validation and enhancement

The MANOVA is a statistical approach to discovering significant differences among samples when all dependent variables of interest are examined (Stahle and Wold 1990). It is used to examine differences between two or more samples with the assessment of all dependent variables concurrently. It generates a single F-statistic based on Wilks' lambda (λ), which evaluates all descriptors' effects concurrently. A significant MANOVA F-statistic shows that the climate of a zone differs considerably from other zones. In this study, 'rankMANOVA' package in R was used for the MANOVA test, where its result depends on wild bootstrap resampling with test statistics and p value. A p value less than 0.001 indicates significant dissimilarity in climate among the zones.

4 Results

4.1 Formulation of CHELSA combined image

To create RGB composite image, the recent (1979–2013) annual averages of rainfall, T_{max} and T_{min} of CHELSA reanalysis datasets were calculated and rescaled individuality from 0 to 255. Then, the grayscale images were rendered together to form a colored image, as shown in Fig. 5, which visualizes the recent climate of Egypt in a unitless value. The figure shows that the effect of the blue band is greater in the north of Egypt, where rainfall is higher, and vice versa in the south, where rainfall is extremely low.

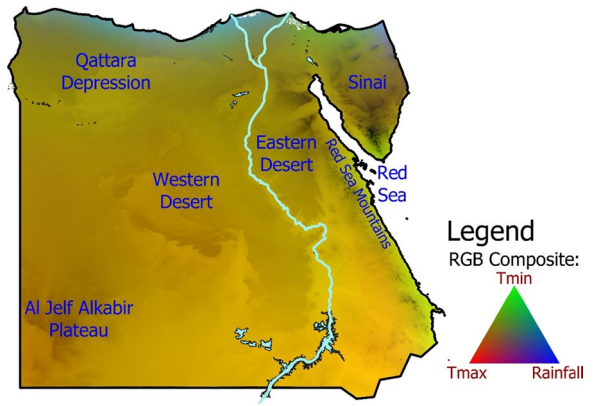

Fig. 5 The rendered RGB image of Egypt's climate

4.2 Image classification results

The SEA was used on the rendered RGB image of Egypt's climate to classify the area into different zones. Climate classification maps for the different number of zones (6, 7, 8 and 9) are presented in Fig. 6. Although using the same number of climate zones, the resulting climate zones differed from previous studies as they do not depend on administrative boundaries. Furthermore, the zoning seems to follow the different climatic variables and elevation distribution. The results showed that the nine climate zones map better represents the climate of Egypt. It could classify the climate of the Saint Catherine area in the Sinai and Suez mountains as a separate zone. The climate of this mountainous region is truly different from other parts of Egypt. This zone was only identified

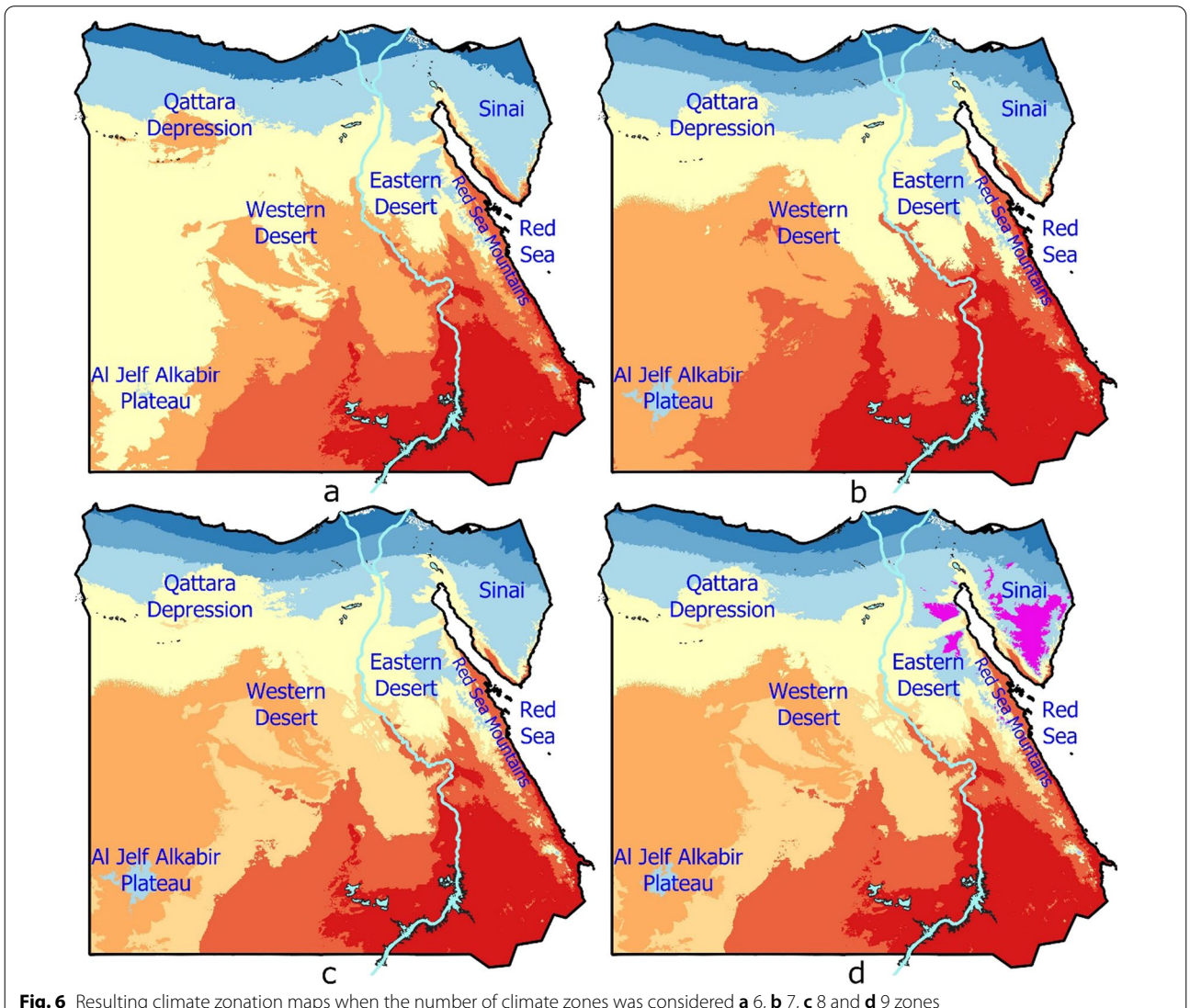

Fig. 6 Resulting climate zonation maps when the number of climate zones was considered **a** 6, **b** 7, **c** 8 and **d** 9 zones

when the number of classes was considered nine. Therefore, the nine climate zones were considered the base for further analysis and merging of climate zones to prepare the final map of Egypt's climate zone.

The PDFs of Tmax, Tmin and rainfall for the nine zones were constructed (Fig. 7) to show each climate zone's characteristics. The highest Tmax and Tmin was noticed in zone 8, followed by zone 7, while the lowest values were noticed in zone 9 for T_{min} and zone 1 and 9 for T_{max}. It is also observed that two pairs of zones, (5 and 6) and (7 and 8), have close T_{max} and T_{min}. The highest annual rainfall was noticed in zone 1, followed by zone 2. Zones 5, 6, 7 and 8 receive low amount of rainfall, as shown in Fig. 7. Table 1 presents each climate zone's average values of the selected nine zones. The average values were similar to the results obtained from the PDFs. The values of zones 5 and 6 were very similar in all three variables. Similar observations can also be made for zones 7 and 8. The mean T_{max} was 30.21 °C for zones 5 and 6 and 33.60 °C for zones 7 and 8. At the

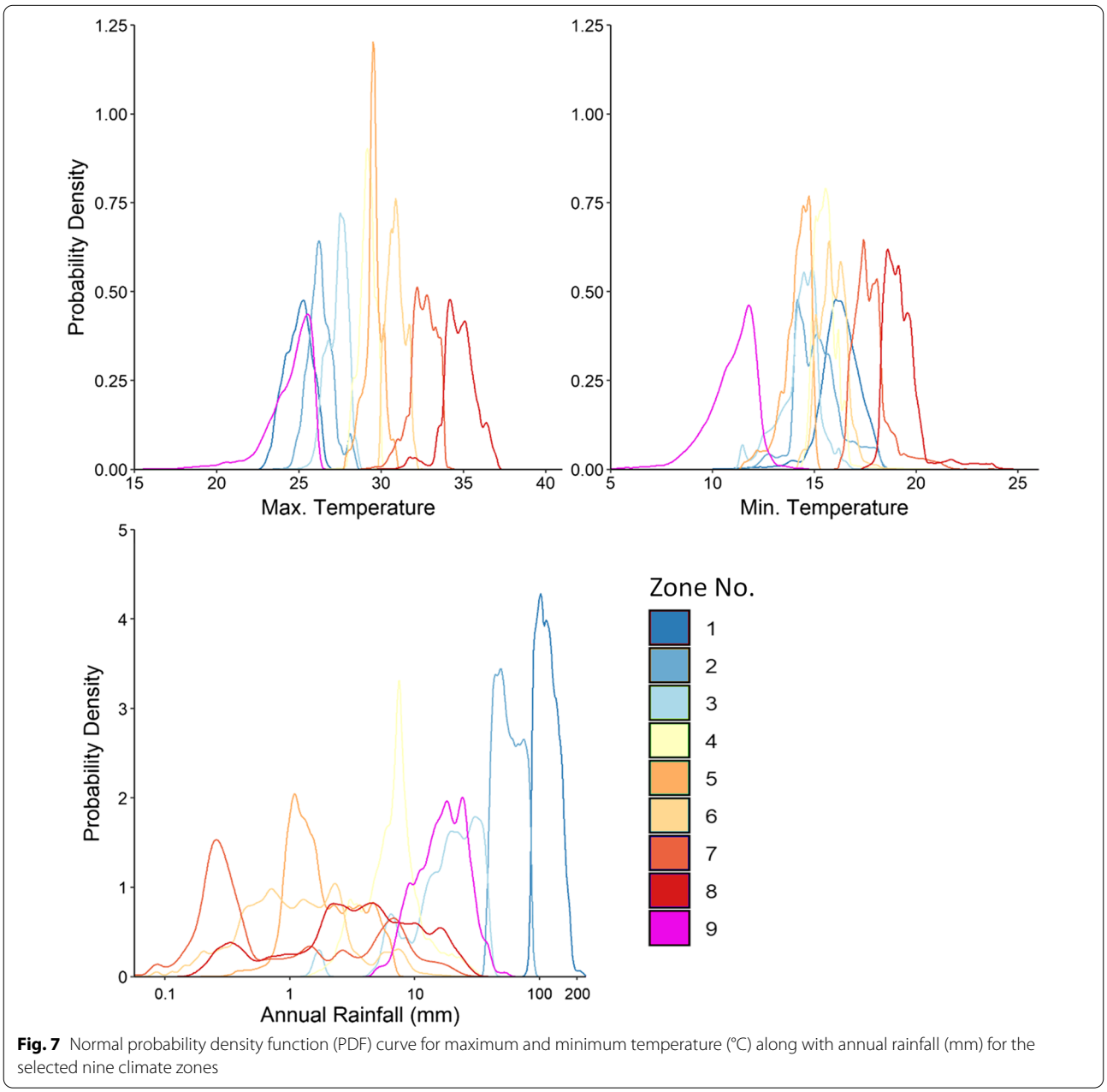

Fig. 7 Normal probability density function (PDF) curve for maximum and minimum temperature (°C) along with annual rainfall (mm) for the selected nine climate zones

Table 1 Average Tmax, Tmin and rainfall for the selected nine climate zones

Zone	Average T_{max} (°C)	Average T_{min} (°C)	Annual rainfall (mm)
1	25.00	16.30	118.30
2	26.10	15.20	58.10
3	27.30	14.30	20.30
4	29.13	15.54	7.55
5	29.52	14.12	2.19
6	30.90	15.88	1.76
7	32.50	17.80	2.60
8	34.75	19.27	5.72
9	24.40	11.00	18.20

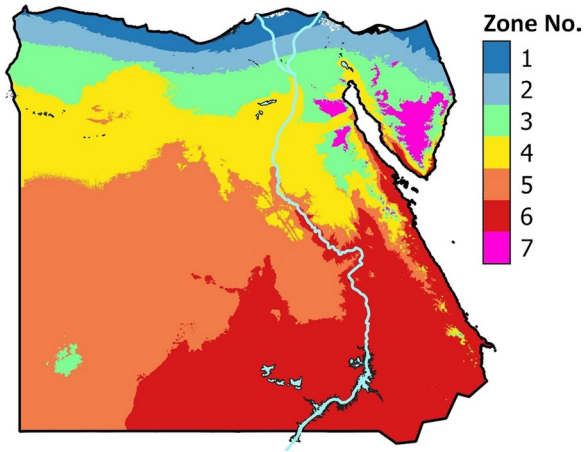

Fig. 8 The seven climate zones of Egypt

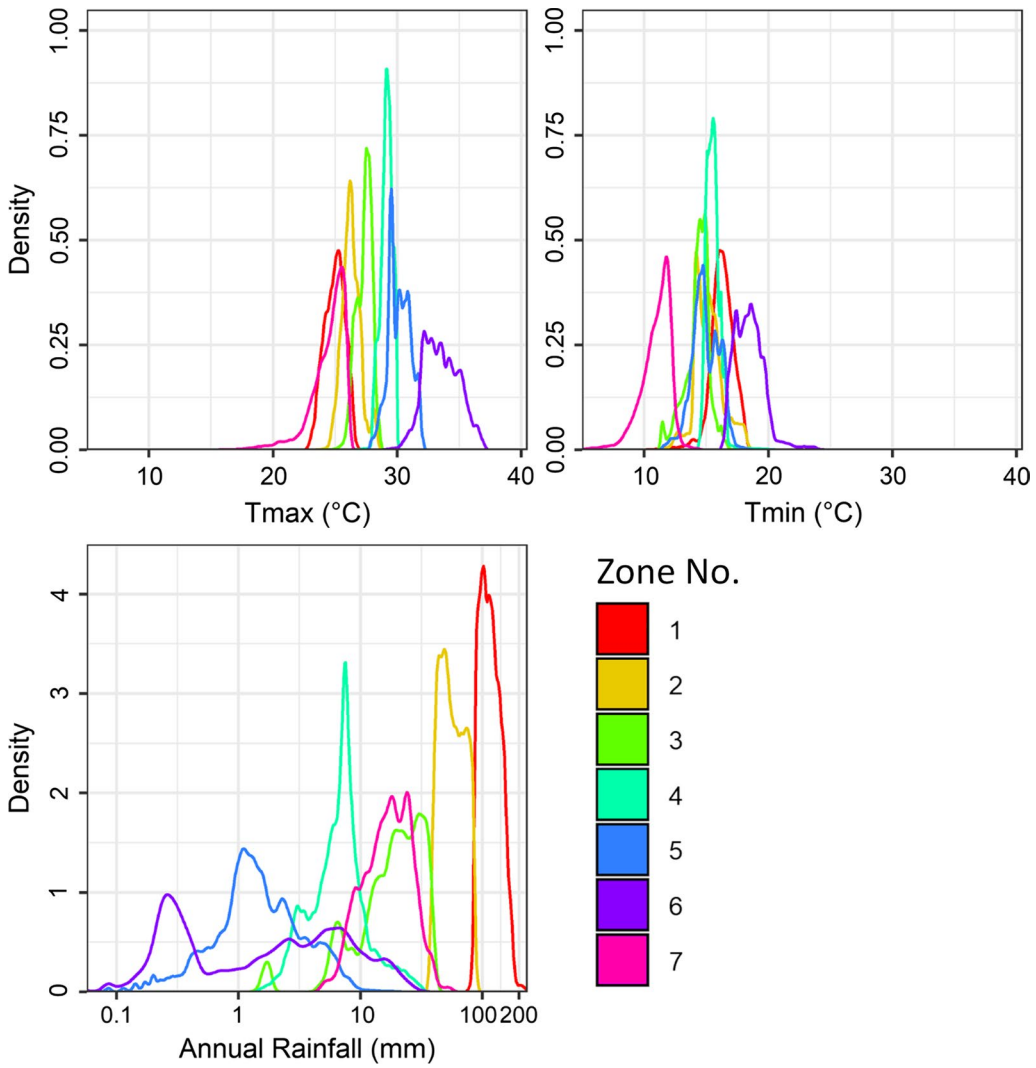

Fig. 9 Normal probability density function (PDF) curve for maximum and minimum temperature (°C) along with annual rainfall (mm) for the selected seven zones

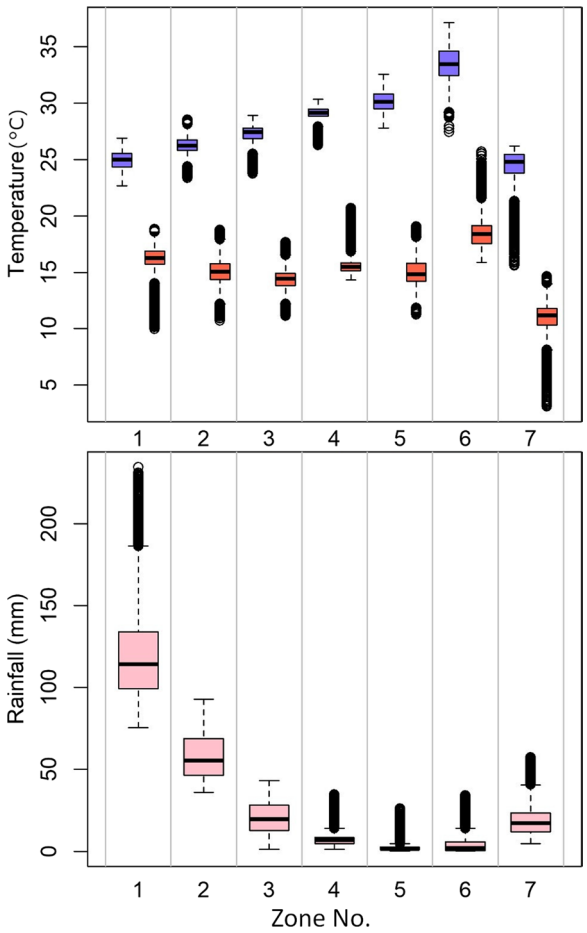

Fig. 10 Box and whisker plots show the maximum (purple) and minimum (orange) temperature (°C) along with annual rainfall (pink) (mm) for the seven climate zones

same time, the mean T_{min} was 15.00 °C for zones 5 and 6 and 18.50 °C for zones 7 and 8. The rainfall for all four zones was less than 6.00 mm/year. Therefore, zones 5 and 6 were merged into a single zone. Similarly, zones 7 and 8 were merged into a single zone.

4.3 Climate zone of Egypt

After merging the two pairs of zones, the climate zones of Egypt are shown in Fig. 8. The rainfall varies between climatic zones due to the terrain and geographical position, which determine the local climate, as shown in Fig. 9. Zone 1 is located on Egypt's north coast, where the rainfall is the highest (118.30 mm) and T_{max} is relatively low (25.00 °C), followed by zone 2, a strip that parallels the Mediterranean Sea, which receives the second-highest rainfall (58.10 mm) and T_{max} of 26.10 °C and T_{min} of 15.20 °C. The rainfalls of zones 3 and 7 were similar (19.00 mm), but T_{max} and T_{min} were less in zone 7 (24.40 and 11.00 °C, respectively) than in zone 3 due to their higher elevations. Zones 5 and 6 experience the lowest rainfall due to their inland location in the south of Egypt. Zone 6 has the highest T_{max} and T_{min} due to its location in the south and southeast of the study area.

Figure 10 shows the annual average of T_{max}, T_{min} and the total rainfall for the seven climate zones using box and whisker plots. The upper chart contains T_{max} as purple color and T_{min} as orange, while the lower chart presents the annual rainfall as pink color. It is observed that Tmax gradually increased from zone 1 (median 25.00 °C) to zone 6 (median 34.00 °C), while T_{min} remains closely similar (median 14.00–18.00 °C). Both Tmax and Tmin dramatically decreased in zone 7, 24.40 °C and 11.00 °C, respectively. The rainfall mostly occurs in zones 1, 2, 3 and 7, while nearly < 5 mm in other zones. The highest rainfall occurs in zone 1 (median 120.00 mm), followed by zone 2 (median 60.00 mm), zone 3 (median 20.00 mm) and the least in zone 7 (median 19.00 mm).

The seven climatic zones identified in this study are unique compared to previous climate classifications. This classification tried to cover what was missed in earlier classifications, as presented in Sect. 2.2. The rainy strips of zone 1 were much wider and more outlined than the classification presented in Ibrahim et al., (1994). Zone 4 defined Qattara depressions, which all previous zonation methods ignored. Zone 3 covers a part of the Al-Jelf

Table 2 MANOVA test statistic results for different zones with each other

Zone nos.	1	2	3	4	5	6
2	28,528.50					
3	60,794.20	43,519.30				
4	77,554.10	77,553.10	97,694.10			
5	146,415.20	129,210.40	145,796.80	115,796.40		
6	136,163.60	152,597.90	164,993.80	162,276.30	189,559.90	
7	16,188.80	31,911.92	37,515.90	81,622.90	171,622.60	127,626.40

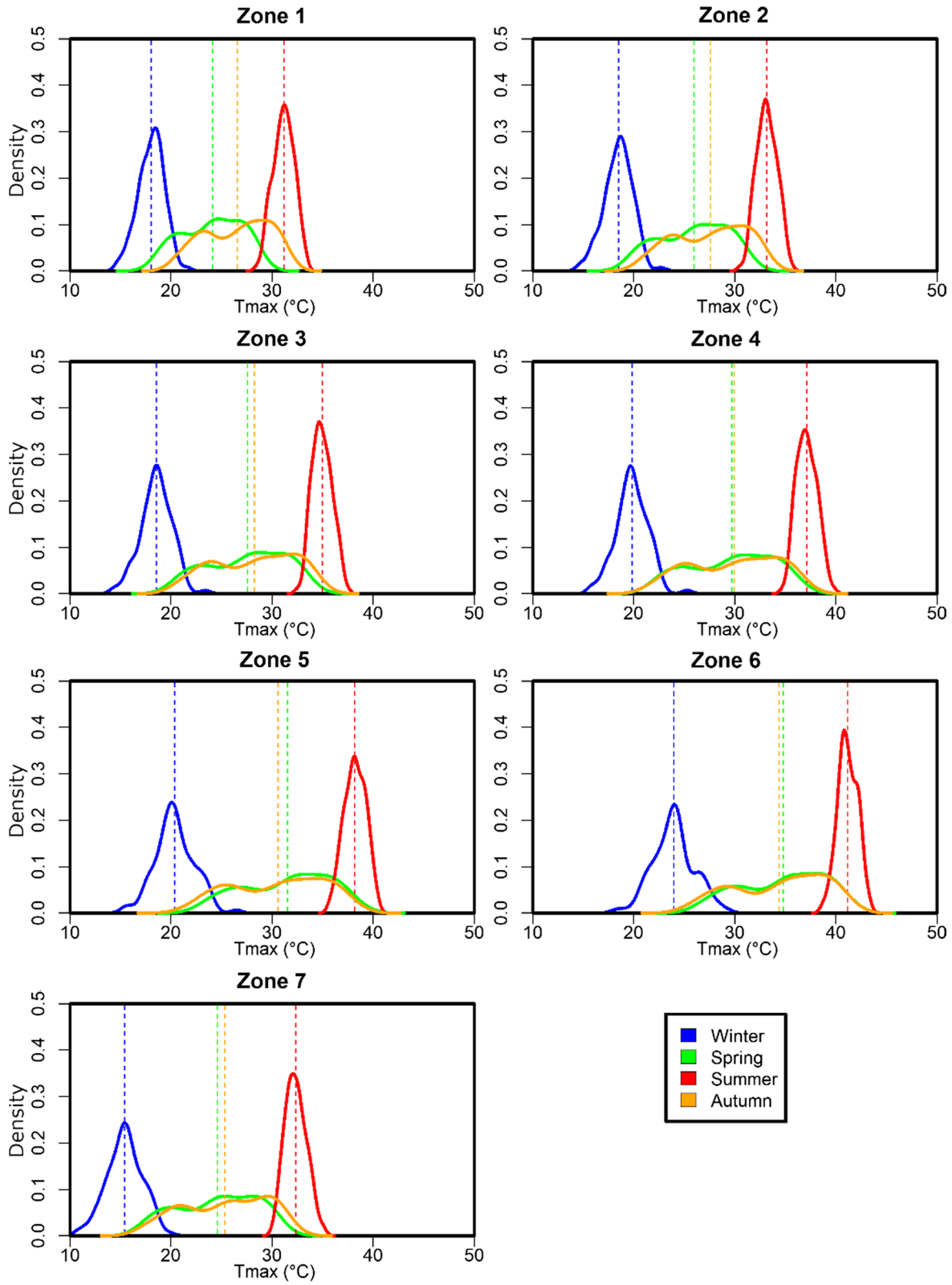

Fig. 11 The probability density function curve of seasonal Tmax (°C) at seven zones

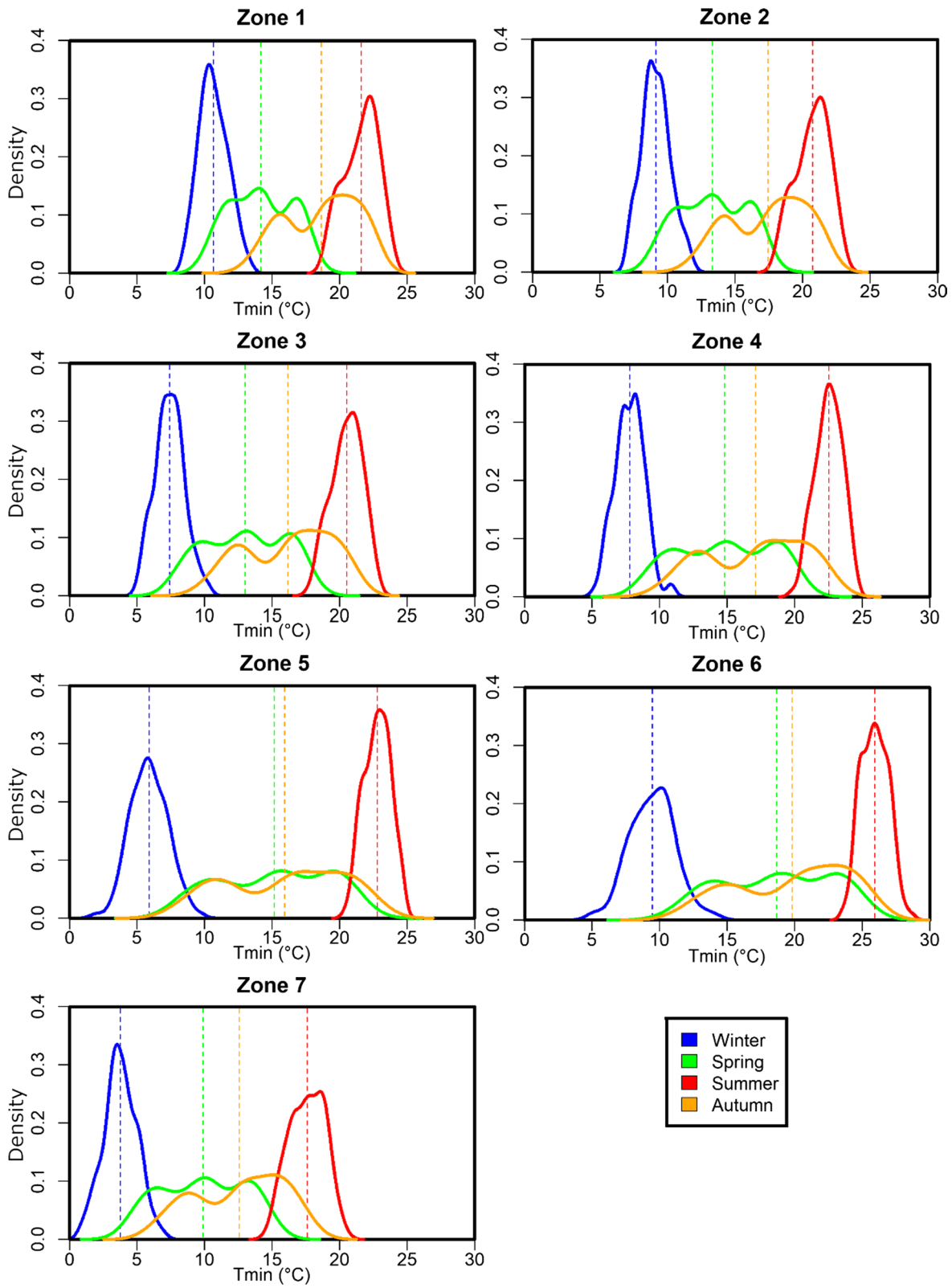

Fig. 12 Same as Fig. 11, but for Tmin

Alkabir Plateau. The zonation process also displayed the chain of Red Sea mountains, the Sinai mountains and the Zaafarana mountains. Although elevation was not considered a predicate in the classification, its effect was clearly visible in the final climate zonation (Fig. 8). This is due to the use of CHELSA data for classification, which has been developed considering elevation as a covariate. Overall, all zones demonstrated reasonable borders of Egypt's climate.

4.4 MANOVA results

The MANOVA test results for different pairs of zones are presented in Table 2. The p values for the statistics were less than 0.001. The p value and test statistics revealed significant dissimilarities between each climate zone. This indicates that each climate zone has its own distinguishable characteristics.

4.5 Seasonal variability

The PDF of Tmax and Tmin for four seasons in each climatic zone is shown in Figs. 11 and 12, respectively. The four seasons include winter (December–February), spring (March–May), summer (June–August) and autumn (September–November). Overall, summer had the highest T_{max} and T_{min} for all zones, while winter had the lowest values. Spring and autumn T_{max} was comparable (medium temperature) for all zones, while autumn T_{min} showed a higher value than spring. The higher autumn T_{min} for zones 1 and 2 was due to their locations near the Mediterranean Sea, while it was due to elevation for zone 7. Zone 6 experiences the highest T_{max} and T_{min} in all seasons, while zone 7 experiences the lowest T_{min} in all seasons.

The quantitative statistics for each climate zone for seasonal and annual T_{max}, T_{min} and rainfall are presented in Supplementary material (Additional file 1: Table S1). There was a distinguishable difference in the coefficient of variance, skewness and kurtosis of the three variables in each climate zone in the seasonal and annual time frames. Sometimes there were some similar results for a single variable, for example, the kurtosis of T_{max} and T_{min} in zones 1 and 2. However, the differences were distinct when the statistics of all variables were considered.

5 Conclusion

A novel image analysis technique is proposed in this study for climate classification based on both temperature and rainfall. The use of high-resolution gridded data enabled a more detailed characterization of Egypt's climate than that was previously possible. The spherical evolution algorithm and statistical analysis classified Egypt's climate into seven zones. Climatic zones are defined by the effect of large-scale climate events and land–sea interactions in and around the study area. The PDF illustrated the different behavior of climatic parameters for each climate zone. The visual inspection also ascertains the ability of the method to distinguish different climate zones, including the small cold zones in the mountainous northeast. Therefore, the climate zonation map generated in this study can be considered reliable. For the first time, the present study established a precise categorization of Egypt's climate, which can aid in the understanding of the physics governing the local climate. Additionally, the reported results can be used by different stakeholders, particularly in climate change research and adaptation, water resource conservation, infrastructure development, agricultural planning and biological conservation. Other climatic factors, such as humidity, evapotranspiration, solar radiation and wind speed, may be incorporated in the future for climate zonation. Besides, other climate datasets, such as WorldClim and TERRA, can be used in the future to quantify uncertainty in climate zonation caused by gridded datasets. The climate zoning presented in this study only represents Egypt's recent climate (1979–2013). It would be fascinating to learn how Egypt's climatic zone has evolved through time and how it may change in the future due to climate change.

Supplementary Information

The online version contains supplementary material available at https://doi.org/10.1186/s40645-022-00494-3.

Additional file 1. Statistics of seasonal and annual time series.

Acknowledgements

The authors thank the three anonymous reviewers for their insightful comments. The authors are thankful to the Swiss Federal Research Institute for providing CHELSA meteorological data.

Author contributions

MMH contributed to formal analysis, investigation, methodology and writing of the original draft. MMH and SS were involved in data curation, investigation and resources. MSN and SS contributed to review and editing. MSN and SS were involved in conceptualization, review and editing. All authors read and approved the final manuscript.

Funding

Open access funding provided by The Science, Technology & Innovation Funding Authority (STDF) in cooperation with The Egyptian Knowledge Bank (EKB). This research did not receive any specific grant from funding agencies in the public, commercial or not-for-profit sectors.

Data availability

A shapefile of the proposed climate zones is available for free at Figshare (https://doi.org/10.6084/m9.figshare.17278256.v1).

Code availability

The code was written using R software, R.3.4, to produce the data. The code is available when requested.

Declarations

Competing interests

The authors declare that they have no known competing financial interests or personal relationships that could influence the work reported in this paper.

Author details

[1]Construction and Building Engineering Department, College of Engineering and Technology, Arab Academy for Science, Technology and Maritime Transport (AASTMT), B 2401 Smart Village, Giza 12577, Egypt. [2]Construction and Building Engineering Department, College of Engineering and Technology, Arab Academy for Science, Technology and Maritime Transport (AASTMT), 2033 Elhorria Heliopolis, Cairo, Egypt. [3]Department of Hydraulics and Hydrology, School of Civil Engineering, Faculty of Engineering, Universiti Teknologi Malaysia (UTM), 81310 Skudia, Johor, Malaysia.

Received: 23 December 2021 Accepted: 8 June 2022
Published online: 17 June 2022

References

Abidi M, Fizazi H, Boudali N (2021) Clustering of remote sensing data based on spherical evolution algorithm. Int Rev Aerosp Eng IREASE 14(2). https://www.praiseworthyprize.org/jsm/index.php?journal=irease&amp

Abuzaid AS, Abdelatif AD (2022) Assessment of desertification using modified MEDALUS model in the north Nile Delta, Egypt. Geoderma 405:115400

AFED (2017) Arab environment in 10 Years. In: Saab (ed) Annual report of arab forum for environment and development, Beirut

Badreldin N, Frankl A, Goossens R (2014) Assessing the spatiotemporal dynamics of vegetation cover as an indicator of desertification in Egypt using multi-temporal MODIS satellite images. Arab J Geosci 7(11):4461–75. https://doi.org/10.1007/s12517-013-1142-8

Bailey RG (2009) Applications of ecosystem geography. In: Ecosystem geography, Springer, pp 169–93

Baker B, Diaz H, Hargrove W, Hoffman F (2010) Use of the Köppen-Trewartha climate classification to evaluate climatic refugia in statistically derived ecoregions for the People's Republic of China. Clim Change 98(1–2):113–131

Barbalho FD, da Silva GFN, Formiga KTM (2014) Average rainfall estimation: methods performance comparison in the Brazilian semi-arid. J Water Resour Prot Estados Unidos 6(02):97–103

Belda M, Holtanová E, Halenka T, Kalvová J (2014) Climate classification revisited: from Köppen to Trewartha. Clim Res 59(1):1–13

Bienvenido-Huertas D, Marín-García D, Carretero-Ayuso MJ, Rodríguez-Jiménez CE (2021) Climate classification for new and restored buildings in andalusia: analysing the current regulation and a new approach based on k-means. J Build Eng 43:102829. https://doi.org/10.1016/j.jobe.2021.102829

Collins JA, Prange M, Caley T, Gimeno L, Beckmann B, Mulitza S et al (2017) Rapid termination of the African Humid Period triggered by northern high-latitude cooling. Nat Commun 8(1):1372

El Kenawy AM, Mccabe MF (2016) A multi-decadal assessment of the performance of gauge- and model-based rainfall products over Saudi Arabia: climatology, anomalies and trends. Int J Climatol 36(2):656–674

El-Geziry TM, Dabbous ASED, Abdallah AM, Eid FM (2021) Temporal variability of sea-level in Safaga Harbour, Egypt in relation with meteorological conditions and tidal characteristics. Arab J Geosci 14(13):1206. https://doi.org/10.1007/s12517-021-07561-x

Elmallah ES, Elsharkawy SG (2011) Influence of circulation indices upon winter temperature variability in Egypt. J Atmos Solar Terr Phys 73(4):439–48

El-Ramly IM (1965) Contributions to hydrogeological study of limestone terrains in UAR. In: Proceedings of symposium on. fracture rocks, Dubrovnik, pp 348–77

Fávero LP, Belfiore P (2019) Data science for business and decision making. In: Press A (ed), Elsevier

Feddema JJ (2005) A revised thornthwaite-type global climate classification. Phys Geogr 26(6):442–466

Gad A (2020) Qualitative and quantitative assessment of land degradation and desertification in egypt based on satellite remote sensing: urbanization, salinization and wind erosion. In: Elbeih SF, Negm AM, Kostianoy A (eds) Environmental remote sensing, Egypt, Springer International Publishing, Cham, pp 443–97. https://doi.org/10.1007/978-3-030-39593-3_15

Gado TA, El-Agha DE (2020) Feasibility of rainwater harvesting for sustainable water management in urban areas of Egypt. Environ Sci Pollut Res 27(26):32304–17

Gado TA, El-Agha DE (2021) Climate change impacts on water balance in Egypt and opportunities for adaptations. In: Abu-hashim M, Khebour Allouche F, Negm A (eds), Agro-environmental sustain. MENA Reg. [Internet]. Cham: Springer International Publishing, pp 13–47. https://doi.org/10.1007/978-3-030-78574-1_2

Geiger R (1954) Landolt–Börnstein–Zahlenwerte und Funktionen aus Physik, Chemie, Astronomie, Geophysik und Technik, alte Serie, vol 3, Ch. Klassif. der Klimate nach W. Köppen, Springer, Berlin, pp 603–607

Hamed MM, Nashwan MS, Shahid S (2021) Performance evaluation of reanalysis precipitation products in Egypt using fuzzy entropy time series similarity analysis. Int J Climatol 41(11):5431–46. https://doi.org/10.1002/joc.7286

Hamed MM, Nashwan MS, Shahid S (2022a) novel selection method of CMIP6 GCMs for robust climate projection. Int J Climatol. https://doi.org/10.1002/joc.7461

Hamed MM, Nashwan MS, Shahid S, Ismail T, Wang X, Dewan A et al (2022b) Inconsistency in historical simulations and future projections of temperature and rainfall: a comparison of CMIP5 and CMIP6 models over Southeast Asia. Atmos Res 265:105927

Hamed MM, Nashwan MS, Shahid S (2022c) Inter-comparison of historical simulation and future projection of rainfall and temperature by CMIP5 and CMIP6 GCMs over Egypt. Int J Climatol. https://doi.org/10.1002/joc.7468

Haque MM, Egodawatta P, Rahman A, Goonetilleke A (2015) Assessing the significance of climate and community factors on urban water demand. Int J Sustain Built Environ 4(2):222–30

Hasanean HM (2004) Wintertime surface temperature in Egypt in relation to the associated atmospheric circulation. Int J Climatol 24(8):985–99. https://doi.org/10.1002/joc.1043

HBRC (2006) The Egyptian code for enhancing energy use in buildings, Housing and Building Research Center (HBRC), Cairo, Egypt

Hubalek Z, Horakova M (1988) Evaluation of climatic similarity between areas in biogeography. J Biogeogr 15(3):409–18

Hwang SH, Ham DH (2013) Quantitative evaluation for regional vulnerability of precipitation networks. J Korean Soc Hazard Mitig 13(5):169–83

Ibrahim YAE, Nasr NE-S, Ghalab ME-S, Abd El-Hakim MS (1994) Geography of Egypt (in Arabic). Egypt: General Egyptian Organization for Books

Karger DN, Conrad O, Böhner J, Kawohl T, Kreft H, Soria-auza RW et al (2017) Climatologies at high resolution for the earth's land surface areas. Sci Data 4:1–20

Kaufman L, Rousseeuw PJ (2009) Finding groups in data: an introduction to cluster analysis. Wiley, New York

Kelley OA (2014) Where the least rainfall occurs in the Sahara desert, the TRMM radar reveals a different pattern of rainfall each season. J Clim 27(18):6919–6939

Köppen WP (1936) Das geographische system der Klimate: Mit 14 Textfiguren, Borntraeger

Kottek M, Grieser J, Beck C, Rudolf B, Rubel F (2006) World map of the Köppen-Geiger climate classification updated. Meteorol Z 15(3):259–63. https://doi.org/10.1127/0941-2948/2006/0130

Lee JH, Byun H, Kim HS, Jun HD (2013) Evaluation of a raingauge network considering the spatial distribution characteristics and entropy: a case study of Imha dam basin. J Korean Soc Hazard Mitig 13(2):217–26

Morrissey ML, Maliekal JA, Greene JS, Wang J (1995) The uncertainty of simple spatial averages using rain gauge networks. Water Resour Res 31(8):2011–7. https://doi.org/10.1029/95WR01232

Nashwan MS, Shahid S (2019a) Symmetrical uncertainty and random forest for the evaluation of gridded precipitation and temperature data. Atmos Res 230:104631. https://doi.org/10.1016/j.atmosres.2019.104632

Nashwan MS, Shahid S (2019b) Spatial distribution of unidirectional trends in climate and weather extremes in Nile river basin. Theor Appl Climatol 137(1–2):1181–1199

Nashwan MS, Shahid S (2022) Future precipitation changes in Egypt under the 1.5 and 2.0°C global warming goals using CMIP6 multimodel ensemble. Atmos Res 265:105908

Nashwan MS, Shahid S, Abd Rahim N (2019a) Unidirectional trends in annual and seasonal climate and extremes in Egypt. Theor Appl Climatol 136(1–2):457–73
Nashwan MS, Shahid S, Chung E-SS (2019b) Development of high-resolution daily gridded temperature datasets for the central north region of Egypt. Sci. Data 6(1):138. https://doi.org/10.1038/s41597-019-0144-0
Nashwan MS, Shahid S, Wang X (2019c) Assessment of satellite-based precipitation measurement products over the hot desert climate of Egypt. Remote Sens 11(5):555
Nashwan MS (2020) High-resolution gridded climate dataset for data-scarce region, Universiti Teknologi Malaysia
Netzel P (2017) Stepinski TF (2017) World climate search and classification using a dynamic time warping similarity function BT—advances in geocomputation. In: Griffith DA, Chun Y, Dean DJ (eds) Advanced geocomputation. Springer, Cham, pp 181–95
Ouda SAH, Norledin TA (2017) Evapotranspiration data to determine agroclimatic zones in Egypt. J Water I Dev 32(1):79–85
Peel MC, Finlayson BL, McMahon TA (2007) Updated world map of the Köppen-Geiger climate classificatio. Hydrol Earth Syst Sci 11(3):1633–1644
Redolat D, Monjo R, Lopez-Bustins JA, Martin-Vide J (2019) Upper-level mediterranean oscillation index and seasonal variability of rainfall and temperature. Theor Appl Climatol 135(3):1059–77. https://doi.org/10.1007/s00704-018-2424-6
Rubel F, Kottek M (2010) Observed and projected climate shifts 1901–2100 depicted by world maps of the Köppen-Geiger climate classification. Meteorol Z 19(2):135–41. https://doi.org/10.1127/0941-2948/2010/0430
Sa'adi Z, Shahid S, Shiru MS (2021) Defining climate zone of Borneo based on cluster analysis. Theor Appl Climatol 145:1467–84. https://doi.org/10.1007/s00704-021-03701-1
Salehie O, Ismail T, Shahid S, Sammen SS, Malik A, Wang X (2021) Selection of the gridded temperature dataset for assessment of thermal bioclimatic environment changes in Amu Darya River Basin. Stoch Environ Res Risk Assess. https://doi.org/10.1007/s00477-022-02172-8
Salman SA, Shahid S, Ismail T, Al-Abadi AM, Wang X, Chung ES (2019) Selection of gridded precipitation data for Iraq using compromise programming. Meas J Int Meas Conf 132:87–98. https://doi.org/10.1016/j.measurement.2018.09.047
Sánchez-García D, Bienvenido-Huertas D, Pulido-Arcas JA, Rubio-Bellido C (2020) Analysis of energy consumption in different european cities: the adaptive comfort control implemented model (ACCIM) considering representative concentration pathways (RCP) scenarios. Appl Sci 10:1513
Sayed A, Hiroshi Y, Goto T, Enteria N, Radwan MM, Eid MA (2013) An analysis of thermal comfort for indoor environment of the New Assiut Housing in Egypt. Int J Archit Environ Eng 7(5):381–387
Shaltout M, El Gindy A, Omstedt A (2013) Recent climate trends and future scenarios along the Egyptian Mediterranean coast. Geofizika 30(1):19–42
Sharp AL, Owen WJ, Gibbs AE (1961) Comparison of methods of estimating precipitation on watersheds. J Geophys Res Am Geophys Union 66:2559
Sihag P, Esmaeilbeiki F, Singh B, Pandhiani SM (2020) Model-based soil temperature estimation using climatic parameters: the case of Azerbaijan Province, Iran. Geol Ecol Landsc 4(3):203–15. https://doi.org/10.1080/24749508.2019.1610841
Stahle L, Wold S (1990) Multivariate analysis of variance (MANOVA). Chemom Intell Lab Syst 9(2):127–41
Sweed HS (2016) Population ageing-Egypt report. Middle East J Age Ageing 13(2):10–17
Tai APK, Mickley LJ, Jacob DJ (2010) Correlations between fine particulate matter (PM25) and meteorological variables in the United States: implications for the sensitivity of PM25 to climate change. Atmos Environ 44(32):3976–84. https://doi.org/10.1016/j.atmosenv.2010.06.060
Tang D (2019) Spherical evolution for solving continuous optimization problems. Appl Soft Comput J 81:105499. https://doi.org/10.1016/j.asoc.2019.105499
Thornthwaite CW (1948) An approach toward a rational classification of climate. Geogr Rev JSTOR 38(1):55–94. https://doi.org/10.2307/210739
Trewartha GT, Horn LH (1980) An Introduction to climate. McGraw-Hill, New York, p 416
Tsvieli Y, Zangvil A (2007) Synoptic climatological analysis of Red Sea trough and non-Red Sea trough rain situations over Israel. Adv Geosci 12:137–143
Xiong J, Yao R, Grimmond S, Zhang Q, Li B (2019) A hierarchical climatic zoning method for energy efficient building design applied in the region with diverse climate characteristics. Energy Build 186:355–67. https://doi.org/10.1016/j.enbuild.2019.01.005
Yanling S, Xiaodonga Y, Deti X (2008) A new method of vegetation–climate classification in China. Int J Climatol 28:1163–1173
Zawadzki II (1973) Errors and fluctuations of raingauge estimates of areal rainfall. J Hydrol 18(3–4):243–55

Publisher's Note